ent 3D image plane lies. With the geometry shown in Fig. 1, A and B, the scanning lines would be seen to lie at level b–b'. They can easily be placed outside the apparent volume in which the 3D optical model lies by overlapping the stack images in a plane outside that volume.

Regarding potential areas of application, this method may be useful where 3D interrelations are too difficult to comprehend by simple through-focusing, where analysis by tracing in serial sections or by camera lucida drawing may be too time consuming (as in the study of sections of central nervous system tissue; Figs. 2 and 4), or where serial sectioning or grinding is not allowed because the intrinsic or scientific value of the specimen is too high (as in the study of archaeological jewels or fossils).

References and Notes

1. M. Minsky, U.S. patent 3013467 (1961).
2. T. Wilson, *Scanning* **7**, 79 (1985).
3. _____ and C. J. R. Sheppard, *Theory and Practice of Scanning Optical Microscopy* (Academic Press, London, 1984).
4. H. T. M. van der Voort *et al.*, *Scanning* **7**, 66 (1985).
5. M. D. Egger and M. Petran, *Science* **157**, 305 (1967).
6. M. Petran, M. Hadravsky, M. D. Egger, R. Galambos, *J. Opt. Soc. Am.* **58**, 661 (1968).
7. A. Boyde and S. A. Reid, *Bone*, in press.
8. A. Boyde, *Proc. R. Microsc. Soc.* **20**, 131 (1985).
9. M. Petran, M. Hadravsky, A. Boyde, *Scanning* **7**, 97 (1985).
10. R. W. Wijnaendts van Resandt *et al.*, *J. Microsc.* **138**, 29 (1985).
11. A. Boyde and H. F. Ross, *Photogramm. Rec.* **8**, 408 (1975).
12. P. G. T. Howell and A. Boyde, in *Analysis of Organic and Biological Surfaces*, P. Echlin, Ed. (Wiley, New York, 1984), pp. 325–349.

13. I thank the Medical Research Council (United Kingdom) for support and R. Radcliffe and E. Maconnachie for technical and photographic assistance.

2 August 1985; accepted 4 October 1985

Lattice Images of Solid Xenon Precipitates in Aluminum at Room Temperature

Abstract. *Small solid precipitates (bubbles) of xenon in an aluminum matrix have been formed by ion implantation. Lattice images of this room-temperature inert gas solid were obtained using high-resolution phase-contrast electron microscopy. Many bubbles showed a high degree of crystalline perfection, but regions of defective crystallinity were observed in several cases.*

STEPHEN E. DONNELLY
CHRISTOPHER J. ROSSOUW
Division of Chemical Physics, Commonwealth Scientific and Industrial Research Organisation, Clayton, Victoria 3168, Australia

Since the first recognized solidification of argon in 1895 (*1*), inert gas solids have been the object of many experimental and theoretical investigations. Indeed, their simplicity, from the theoretician's point of view, has rendered inert gas solids a useful testing ground for various aspects of solid-state theory (*2*). Because cryogenic or high-pressure techniques (or both) are required to solidify the gases, high-resolution electron microscopy has not hitherto been applied to the rare gas solids. Recently, Templier (*3, 4*) and vom Felde (*5*) and their colleagues have used electron diffraction patterns to identify small solid precipitates of xenon and argon at room temperature in ion-implanted aluminum, and Evans and Mazey (*6*) have made a similar observation of solid krypton in a number of metals.

The identification of these precipitates from clearly identifiable (though weak) diffracted beams suggested to us the possibility of performing high-resolution phase-contrast electron microscopy to produce lattice images of the implanted inert gas precipitates. We now present lattice images of solid xenon precipitates in aluminum at room temperature that show regions of both perfect and defective crystallinity. These lattice images of an inert gas solid demonstrate the potential of the "bubble" as a high-pressure cell for electron microscopy and other studies of rare gas solids. In common with other investigators we continue to use the word "bubbles" to describe inert gas precipitates.

Aluminum films approximately 50 nm thick were prepared by evaporation of aluminum in vacuum onto an air-cleaved {100} NaCl surface heated to about 490 K. This procedure resulted in a polycrystalline film containing grains with preferred <100>, <110>, and <111> orientations. Xenon implantation was carried out with 50-keV Xe^+ ions at a flux of approximately 3×10^{16} ion m^{-2} sec^{-1} to a fluence of 10^{20} ion m^{-2}. The films were irradiated on the NaCl substrates at a temperature of 270 ± 10 K. The projected range of these ions was calculated from an analytical model (*7*) to be 25 ± 4 nm. The sputtering yield (*8*) was such that about 15 nm of aluminum was removed during irradiation. The films were floated off the substrate in distilled water and caught on 400-mesh copper grids. The films were then examined at 200 keV using the high-resolution top-entry stage of a transmission electron microscope (JEOL 200 CX).

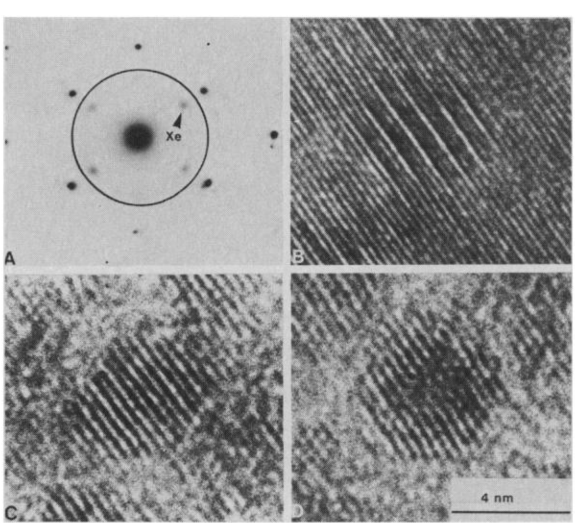

Fig. 1. (A) Diffraction pattern from a <110> aluminum grain. The arrow indicates one of the comparatively weak xenon {111} spots; the circle indicates the size of the 20-μm objective aperture. This aperture excludes the beams diffracted from aluminum from contributing to the image. (B) An image taken with the 50-μm objective aperture, with 0.23-nm {111} aluminum fringes merging with a xenon bubble. Here parallel moiré fringes are evident as an increase in intensity every third fringe spacing. (C) An image taken with a 20-μm objective aperture showing 0.35-nm fringes from {111} xenon planes. (D) An image taken under conditions similar to those for (C), with a defect region in the center of the bubble. Again the fringes are from {111} xenon planes. The scale marker is 4 nm.

Figure 1A shows a diffraction pattern from a <110> grain. As in previous diffraction studies (*3–6*), the diffraction pattern has extra reflections, indicating the presence of epitaxial face-centered cubic (*fcc*) precipitates. These represent spacings that are 1.49 ± 0.01 times the aluminum spacing, consistent with an *fcc* lattice parameter of 0.604 ± 0.04 nm. Dark-field microscopy with the extra reflections confirmed that these beams were excited within the implanted bubbles. Although xenon atoms scatter electrons far more strongly than do aluminum atoms, the atomic density in the xenon bubbles was comparatively low, so that the forward scattering potential for electrons in the aluminum matrix was

1.84 times that in the bubbles. These were thus recognizable in bright field by the usual criterion of contrast reversal on passing from underfocus to overfocus.

Figure 1B is a high magnification image of part of a <110> grain taken with a 50-μm objective aperture, which allowed {111} and {200} reflections from both xenon and aluminum to contribute to the image. The film was tilted so that one-dimensional lattice fringes were formed. Aluminum {111} lattice fringes (0.234 nm), as well as parallel moiré fringes due to the mismatch between {111} aluminum and xenon planes, are visible. The high degree of crystalline perfection apparent in this figure is representative of that observed in many of the bubbles.

Figure 1C is an image from a <110> grain taken with a 20-μm objective aperture (indicated by the circle in Fig. 1A), which allowed only {111} and {200} xenon reflections to contribute to the image and excluded all beams diffracted from the aluminum matrix. Again, because of the tilt of the aluminum film about a <111> direction, systematic row diffraction conditions were operating, resulting in a one-dimensional lattice image from {111} planes within the xenon bubble. The faceted nature of the bubbles is evident in Fig. 1, B and C. Figure 1D is an image formed in the same manner as that in Fig. 1C of a bubble whose crystalline perfection is somewhat disturbed near the center.

An analysis of 130 bubbles exhibiting {111} xenon lattice fringes revealed that, in general, the bubbles were faceted but often irregular in shape, although a number of images were consistent with truncated octahedra. The largest bubble in this population was approximately 8 nm, and the smallest was about 2 nm. By approximating the bubble shapes with circles of equivalent projected area and using the resulting diameters as characteristic dimensions, we obtained a roughly symmetrical distribution of sizes ranging from 1.7 to 6.6 nm (mean, 3.5 nm; standard deviation, 1 nm).

The equilibrium pressure, P, required by a spherical bubble of diameter D to balance its surface free energy is given simply by $P = 4\gamma/D$, where γ is the surface tension. Taking γ for aluminum as 0.95 N m^{-1} and neglecting the (small) surface tension of xenon yielded (for spherical bubbles with the above size distribution) equilibrium pressures ranging from 6 to 22 kbar (mean, ~11 kbar). Taking the *fcc* lattice parameter for xenon as 0.604 nm and extrapolating the isotherms of Anderson and Swenson (*10*) to 300 K, we estimate a pressure of 7 kbar within the xenon bubbles; this indicates that they are close to or somewhat below equilibrium pressure. The absence of strain contrast around the bubbles, when viewed under bright-field diffraction contrast-imaging conditions, is a further indication that the bubble pressure differs by, at most, a few kilobars from equilibrium.

Use of the modified Simon equation (*11*) to estimate the melting temperature of macroscopic xenon with the same density as that in our precipitates yielded an expected melting temperature, T_m, of approximately 430 K. Thus for our room temperature observations, the xenon is at a temperature greater than $\frac{2}{3}T_m$ and may be expected to be sufficiently "hot" to anneal out crystalline imperfections. Indeed, we observed a rapid decrease in intensity in higher order xenon reflections, which is indicative of a large Debye-Waller factor at room temperature. Large mean square displacement of atoms from equilibrium positions may result in high defect mobilities and may account for the high degree of crystalline perfection in many bubbles.

We have demonstrated how ion implantation into a host metal matrix may be used to facilitate lattice imaging of an inert gas solid at high pressure. Indeed, if the imaged reflections represent larger spacings than those available within the host matrix, an objective aperture of suitable diameter may be chosen such that lattice information about the bubble alone is contained in the image (Fig. 1C). Information about the interface between the host lattice and bubble (Fig. 1B) and about crystalline defects within the bubbles themselves (Fig. 1D) is thus accessible. Such information cannot be obtained from electron diffraction patterns alone. For small bubbles, the thermodynamic properties may differ from bulk values because the high ratio of surface area to volume may yield behavior strongly dependent on surface or interface properties. For instance, it may be speculated that superheating may occur if the interfacial xenon atoms, in contact with the aluminum, have a larger effective Debye temperature than that of bulk xenon at these pressures.

References and Notes

1. K. Olszewski, *Philos. Trans. R. Soc. London Ser. A* **186**, 253 (1895).
2. M. L. Klein and J. A. Venables, Eds., *Rare Gas Solids* (Academic Press, London, 1977), vols. 1 and 2.
3. C. Templier *et al.*, *C. R. Acad. Sci. Ser. B* **299**, 613 (1984).
4. C. Templier, R. J. Gaboriaud, H. Garem, *Proceedings of the International Conference on Surface Modification of Materials Using Ion Beams*, Heidelberg, Germany, 1984.
5. A. vom Felde, J. Fink, Th. Muller-Heinzerling, J. Pfluger, B. Scheerer, G. Linker, D. Kaletta, *Phys. Rev. Lett.* **53**, 922 (1984).
6. J. H. Evans and D. J. Mazey, *J. Phys. F* **15**, L1 (1985).
7. J. P. Biersack and J. F. Ziegler, *Ion Implantation Techniques*, H. Ryssel and H. Glawischnig, Eds. (Springer-Verlag, Berlin, 1982), pp. 157–170.
8. H. H. Andersen and H. L. Bay, *Sputtering by Particle Bombardment*, R. Behrisch, Ed. (Springer-Verlag, Berlin, 1981), vol. 1, pp. 145–209.
9. M. Rühle and M. Wilkens, *Cryst. Lattice Defects* **6**, 129 (1975).
10. M. S. Anderson and C. A. Swenson, *J. Phys. Chem. Solids* **36**, 145 (1975).
11. R. K. Crawford, in *Rare Gas Solids*, M. L. Klein and J. A. Venables, Eds. (Academic Press, London, 1977), vol. 1, pp. 663–822.

12. We thank R. Bartlett and R. Lamb for technical assistance, A. F. Moodie and P. R. Taylor for fruitful discussion of many aspects of this work, and J. S. Williams for use of the facilities at the Royal Melbourne Institute of Technology.

20 May 1985; accepted 5 August 1985

α_2-Adrenergic Mechanisms in Prefrontal Cortex Associated with Cognitive Decline in Aged Nonhuman Primates

Abstract. *This study provides evidence that the α_2-adrenergic receptor agonist clonidine ameliorates the cognitive deficits exhibited by aged nonhuman primates through drug actions at α_2 receptors. Furthermore, pharmacological profiles in animals with lesions restricted to the dorsolateral prefrontal cortex indicate that this area may be the site of action for some of clonidine's beneficial effects. These results demonstrate that α-adrenergic systems contribute to cognitive function and suggest a new strategy for treating memory disorders in aged humans.*

AMY F. T. ARNSTEN
PATRICIA S. GOLDMAN-RAKIC
Section of Neuroanatomy,
Yale Medical School,
New Haven, Connecticut 06510

Most research on age-related cognitive disorders has emphasized the loss of cholinergic neuronal function (*1*), thus focusing studies of possible pharmacological "replacement therapy" on cholinergic drugs. However, studies of Alzheimer's patients and aged nonhuman primates have found little therapeutic value for indirectly acting cholinergic agonists, and directly acting agonists have had reliable, but limited, beneficial effects (*2*). This may be attributed in part to the complexity of degenerative processes in the aging brain, which include not only loss of cholinergic neurons but deterioration of other neurotransmitter